

MIT Open Access Articles

DERIVING STELLAR EFFECTIVE TEMPERATURES OF METAL-POOR STARS WITH THE EXCITATION POTENTIAL METHOD

The MIT Faculty has made this article openly available. *Please share* how this access benefits you. Your story matters.

Citation: Frebel, Anna, Andrew R. Casey, Heather R. Jacobson, and Qinsi Yu. "DERIVING STELLAR EFFECTIVE TEMPERATURES OF METAL-POOR STARS WITH THE EXCITATION POTENTIAL METHOD." *The Astrophysical Journal* 769, no. 1 (May 20, 2013): 57.

As Published: <http://dx.doi.org/10.1088/0004-637x/769/1/57>

Publisher: Institute of Physics Publishing

Persistent URL: <http://hdl.handle.net/1721.1/88425>

Version: Author's final manuscript: final author's manuscript post peer review, without publisher's formatting or copy editing

Terms of use: Creative Commons Attribution-Noncommercial-Share Alike



DERIVING STELLAR EFFECTIVE TEMPERATURES OF METAL-POOR STARS WITH THE EXCITATION POTENTIAL METHOD¹

ANNA FREBEL², ANDREW R. CASEY^{3,2}, HEATHER R. JACOBSON², QINSI YU²

Draft version April 10, 2013

ABSTRACT

It is well established that stellar effective temperatures determined from photometry and spectroscopy yield systematically different results. We describe a new, simple method to correct spectroscopically derived temperatures (“excitation temperatures”) of metal-poor stars based on a literature sample with $-3.3 < [\text{Fe}/\text{H}] < -2.5$. Excitation temperatures were determined from Fe I line abundances in high-resolution optical spectra in the wavelength range of ~ 3700 to ~ 7000 Å, although shorter wavelength ranges, up to 4750 to 6800 Å, can also be employed, and compared with photometric literature temperatures. Our adjustment scheme increases the temperatures up to several hundred degrees for cool red giants, while leaving the near-main-sequence stars mostly unchanged. Hence, it brings the excitation temperatures in good agreement with photometrically derived values. The modified temperature also influences other stellar parameters, as the Fe I-Fe II ionization balance is simultaneously used to determine the surface gravity, while also forcing no abundance trend on the absorption line strengths to obtain the microturbulent velocity. As a result of increasing the temperature, the often too low gravities and too high microturbulent velocities in red giants become higher and lower, respectively. Our adjustment scheme thus continues to build on the advantage of deriving temperatures from spectroscopy alone, independent of reddening, while at the same time producing stellar chemical abundances that are more straightforwardly comparable to studies based on photometrically derived temperatures. Hence, our method may prove beneficial for comparing different studies in the literature as well as the many high-resolution stellar spectroscopic surveys that are or will be carried out in the next few years.

Subject headings: stars: fundamental parameters — stars: abundances — stars: Population II

1. INTRODUCTION

Determining the atmospheric parameters of a star is fundamental to characterizing and understanding its nature and evolutionary state. These parameters are the effective temperature T_{eff} , surface gravity $\log g$, metallicity $[\text{M}/\text{H}]$ and for 1D abundance analyses also the microturbulent v_{mic} . Particularly, the temperature can be determined with several methods, such as from photometric colors, flux calibrated low-resolution spectra, the shape of the Balmer lines in a high-resolution stellar spectrum and through forcing no trend of Fe I absorption line abundances with the excitation potential of the lines (“excitation balance”), also from high-resolution spectra. The most common technique is to employ broadband colors, with many color-temperature calibrations available for main-sequence stars (e.g., Alonso et al. 1996; Casagrande et al. 2010) and giants (e.g., Alonso et al. 1999) based on the infrared flux method (IRFM). Precise photometry, reliable reddening values and metallicity information are necessary when using this method. Using flux-calibrated low-resolution spectra to measure the strength of the Balmer jump and comparing the spectral shape to grids of synthetic flux spectra is less common (Bessell 2007).

In the absence of photometry or stellar libraries, or to test systematic temperature uncertainties, temperatures can also be obtained from high-resolution spectroscopy alone. Fitting the shape of the Balmer lines with synthetic spectra of known stellar parameters yields temperatures, especially for the warmer main-sequence stars and subgiants (e.g., Barklem et al. 2002). Finally, another commonly used method is to employ Fe I lines throughout the stellar spectrum and force their abundances to show no trend with the excitation potential of each line. Compared to using photometry to derive temperatures, no reddening information is needed for this technique or the Balmer line fitting method. But in turn, high-resolution spectra with resolving power of $R \gtrsim 15,000$ are required, preferably with large wavelength coverage throughout the optical range. A list of Fe absorption lines covering a large range of excitation potentials is also needed.

The different methods are known to produce temperatures with systematic offsets from each other. The “excitation temperatures” are thereby known to yield lower effective temperatures than photometry-based color-temperature calibrations, often by a few hundred degrees. Stars on the upper red giant branch are most affected. Johnson (2002) found their 23 metal-poor giants to be 100 to 150 K cooler when using the excitation method over several color-temperature calibrations. Similar results have been reported by Cayrel et al. (2004), Aoki et al. (2007) Lai et al. (2008), Frebel et al. (2010), Hollek et al. (2011), and many others. The approaches and dealings with this issue have been varied, though.

¹ This paper includes data gathered with the 6.5 meter Magellan Telescopes located at Las Campanas Observatory, Chile.

² Kavli Institute for Astrophysics and Space Research and Department of Physics, Massachusetts Institute of Technology, 77 Massachusetts Avenue, Cambridge, MA 02139, USA

³ Research School of Astronomy & Astrophysics, The Australian National University, Weston, ACT 2611, Australia

Cayrel et al. (2004) reached good agreement between their photometrically derived temperatures and excitation temperatures after they excluded strong lines with excitation potential of $EP = 0$ eV. These often appear to have higher abundances than lines with higher excitation potential. As a consequence, forcing no trend in line abundances with excitation potential can yield artificially cooler temperatures. While a similar approach (cutting $EP < 0.2$ eV) worked for Cohen et al. (2008), it did not yield the same outcome for Lai et al. (2008) and Hollek et al. (2011). With or without cutting low- EP lines, the latter two studies found significant trends of abundance with excitation potential to remain. Consequently, different authors have adopted either spectroscopic temperatures, or the photometric ones, or tried to find a middle ground between the results of the two techniques.

The situation is further complicated by the fact that different model atmosphere codes have been used over time, producing different results leading to and possibly increasing the differences between spectroscopic and photometric temperatures. For example, using a model code that treated scattering as true absorption Cayrel et al. (2004) found larger discrepancies than when using codes that treated scattering as Rayleigh scattering.

However, recently, Hollek et al. (2011) carried out an abundance analysis of 16 metal-poor giants using different versions of the MOOG code (Snedden 1973). They found that if scattering is properly treated, the temperatures were generally even lower than in an older MOOG version that treated scattering as true absorption – the opposite of what was found by Cayrel et al. (2004) (although they make no quantitative statement about the magnitude of the effect and how it compares to their proper-scattering treatment when not excluding lines with $EP < 1.2$ eV).

This study aims at empirically resolving the issue of producing lower spectroscopic excitation temperatures when employing the latest version of the widely-used MOOG code that now properly treats the scattering (Sobeck et al. 2011). We provide simple corrections to the slope of the Fe I abundances as a function of excitation potential for metal-poor stars that bring the excitation temperatures in rough agreement with photometrically derived values. This way, we can use “the best of both worlds”: not depending on photometry, reddening and color-temperature relations, while obtaining temperatures and hence chemical abundances that can be easily and relatively fairly compared to results based on photometric temperatures. Our pragmatic approach does not resolve the underlying processes that likely cause the temperature discrepancies which seem to be manifold (scattering treatments in codes, line formation of low and high- EP lines, wavelength coverage of lines and data quality, effects due to non-local thermodynamic equilibrium, etc.) but at least it provides a means to facilitate a more homogeneous analysis of stars that have temperatures derived from different methods. Much work has been invested in improving photometric temperature scales. For example, using the IRFM method, Casagrande et al. (2010) showed this photometric temperature determination method to be hardly sensitive to theoretical model parameters, especially the surface gravity and metallicity (particularly for extremely

metal-poor stars). The uncertainty with respect to their zero-point (well-calibrated, against interferometric angular diameter measurements and HST spectroscopy) using solar twins is 15 K, whereas their final IRFM effective temperatures have typical uncertainties ranging from 60 to 90 K for metal-poor stars and slightly lower values for more metal-rich stars. The independence of metallicity when deriving temperatures this way makes the IRFM method, in principle, the preferred one for low-metallicity stars. The only major caveat would be that the IRFM method sensitively depends on very accurate reddening values, as an 0.01 mag change in $E(B-V)$ leads to ± 50 K change in the final temperature.

Given these facts, it appears timely to bring the somewhat plagued excitation temperatures onto a comparable scale. Another reason for such a “re-calibration” is that the stellar surface gravities, usually derived through the Fe I-Fe II ionization equilibrium, depend on the derived temperatures. With lower temperatures, lower gravities are derived. Hence, in many cases of cool giants, much too low gravities have been obtained (compared with isochrones and parallax-derived values), to a point that they become unphysical. This effect is particularly pronounced in metal-poor stars with lower S/N spectra which leave few Fe II to be measured (e.g., see Table 5 in Hollek et al. (2011)). In the same way, if only primarily strong lines are measurable in the spectrum, the microturbulent velocity becomes very large, often past 2.5 km s^{-1} . Especially, metal-poor stars in dwarf galaxies have been affected by this, since they are all bright giants and the data quality is often rather poor given their faint apparent magnitudes (McWilliam et al. 1995; Koch et al. 2008; Aoki et al. 2009; Hollek et al. 2011; Simon et al. 2010).

In summary, adjusting the spectroscopic temperatures leads to improved stellar parameters, at least in the metal-poor regime and particularly for metal-poor giants with $[\text{Fe}/\text{H}] < -2.0$. Broadly adopting this scheme may prove beneficial for the many high-resolution spectroscopic surveys (Gaia-ESO, GALAH) that will soon provide large amounts of stellar spectra that have to be analysed homogeneously and consistently.

2. “CALIBRATION” SAMPLE AND ABUNDANCE ANALYSIS

We chose seven metal-poor stars with metallicities of $-3.3 < [\text{Fe}/\text{H}] < -2.5$ and spanning the largest possible temperature range from 4600 to 6500 K covering warm main-sequence to cool giants to investigate systematic differences between the excitation temperatures and photometric temperatures.

All high S/N , high-resolution spectra were obtained with the MIKE spectrograph (Bernstein et al. 2003) on the Magellan-Clay telescope at Las Campanas Observatory between 2009 and 2011. An $0''.7$ slit width was used resulting in a resolving power of $R \sim 35,000$ in the blue and $\sim 28,000$ in the red spectral range. MIKE spectra cover nearly the full optical wavelength range of 3350–9100 Å, although the S/N is low below 3700 Å. The reduced spectra were normalized, the orders merged and then radial velocity corrected. The S/N ratio of the final spectra ranges from 70 to 300 at ~ 4100 Å, and from 70 to 500 at ~ 6700 Å per pixel.

Equivalent widths were measured by fitting Gaussian

profiles to the absorption lines. For a metal line list we used the list described in Roederer et al. (2010). Between ~ 50 and ~ 230 FeI and 2 and 26 FeII lines were measured in each sample star. See Table 1 for the lines used and their measured equivalent widths, although we only list lines with reduced equivalent widths of $\gtrsim -4.5$. In Figure 1 we furthermore show a comparison of the ~ 200 equivalent width measurements of HD122563 common to our lines and those of Aoki et al. (2007) and Cayrel et al. (2004). Not all our lines were measured by these two studies, but those that are in common agree very well with each other. The agreements of our measurements are 0.20 ± 0.16 mÅ and 0.25 ± 0.28 mÅ, respectively, so no significant offsets exist between the three data sets.

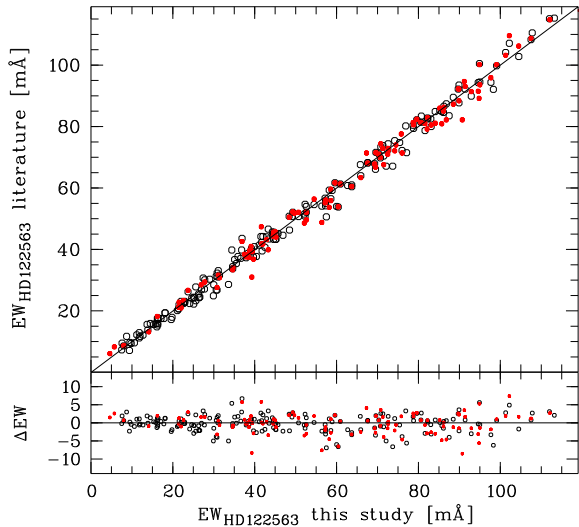


FIG. 1.— Comparison of equivalent width measurements for HD122563 of this study with those of Aoki et al. (2007) (black open circles) and Cayrel et al. (2004) (red filled circles). The agreement is excellent.

For our 1D LTE abundance analysis, we used model atmospheres from Castelli & Kurucz (2004) and the MOOG analysis code of Sneden (1973), albeit the latest version that appropriately treats scattering as Rayleigh scattering and not as true absorption as done in previous versions (Sobeck et al. 2011). The metal line abundances are presented in Table 1. Our study about stellar parameter determinations is based on equivalent width measurements of Fe lines between 3700 and 7000 Å.

3. ADJUSTING THE “EXCITATION TEMPERATURE” SCALE

We used our sample of well-studied stars to produce a straight-forward method of adjusting the excitation temperature scale in order to arrive at spectroscopic temperatures that agree with photometric ones. After measuring the equivalent widths we first determined the stellar temperatures by forcing no trend of the abundances of individual FeI lines as a function of their excitation potential. In the process we varied the microturbulent velocity to produce no trend of the line abundances with reduced equivalent widths. Simultaneously, to determine the surface gravity, the FeII abundance was matched to the FeI abundance. Finally, another

input parameter of the model atmosphere is the metallicity $[m/H]$ of the star. We use a general prescription of $[m/H] = [Fe/H] + 0.25$ to account for the overabundances of α -elements of $[\alpha/Fe] \sim 0.3$ as well as small overabundances of carbon and/or oxygen ($[C,O/Fe] \sim 0.3$) which are all typical for metal-poor halo stars.

We then carried out an extensive literature search to assess the range of photometric temperatures determined for each star. Table 2 shows a representative range of values found in the literature, including the colors and the color-temperature relations used for their calculation. For comparison, we also include T_{eff} values calculated using the IRFM method in recent works whose color-temperature relations are commonly used (e.g., Alonso et al. 1996, 1999, Casagrande et al. 2010). For two stars, CD-24 17504 and G64-12, we found relatively few photometrically derived values, and most where done using older temperature calibrations. We thus calculated photometric temperatures ourselves, based on literature photometry and reddening values and using the Casagrande et al. (2010) scale. Finally, for HE 1523-0901, only one photometric temperature is available (Frebel et al. 2007a) but at least it was an average based on six different colors.

As can be seen, temperature ranges of several hundred degrees were found for some cases, making it difficult to assess which individual temperatures would be “the best”. Hence, we resorted to choosing “common sense” values, as our original aim was to re-calibrate our excitation temperature scale to a level common with that of photometric temperatures found using the more recent color-temperature relations. Our initial excitation temperatures and associated adopted literature values (based on photometry) are listed in Table 3. We stress that the photometric temperatures we have adopted are not strictly averages of the values listed in Table 2, rather they are appropriate near-median quantities from the range of values found by multiple authors using different color-temperature relations and photometry.

Figure 2 (upper panel) then shows the differences in effective temperatures between our initial excitation temperatures and our adopted literature values as a function of the initial temperatures. We find a strong, linear relation, with the largest differences at the cooler temperatures of upper red giant branch stars. An (unweighted) least-square regression yields the following relation:

$$T_{\text{eff,corrected}} = T_{\text{eff,initial}} - 0.1 \times T_{\text{eff,initial}} + 670 \quad (1)$$

This temperature dependent behavior is completely in line with the vast majority of previous studies that reported differences between spectroscopic and photometric temperatures of several hundred degrees, as most analyzed star were giants. However, main-sequence stars are hardly affected, as we find essentially the same temperatures. We also overplot nominal error bars of 134 K which reflect typical uncertainties in temperature determinations (60 K for photometric and 120 K for spectroscopic values).

Since we adopted common sense representative photometric temperatures from the literature that are based on a variety of colors and color-temperature relations, we also attempted to calculate temperatures ourselves, for an exemplary color, $V - K$, and using the Alonso et al.

TABLE 1
EQUIVALENT WIDTHS AND METAL LINE ABUNDANCES OF STARS IN THE CALIBRATION SAMPLE

λ [Å]	Species	χ [eV]	$\log gf$ [dex]	HD122563		HE 1523–0901		BD–18 5550		CS22892–052		HD140283		CD–24 17504	
				EW [mÅ]	$\log \epsilon(X)$ [dex]	EW [mÅ]	$\log \epsilon(X)$ [dex]	EW [mÅ]	$\log \epsilon(X)$ [dex]	EW [mÅ]	$\log \epsilon(X)$ [dex]	EW [mÅ]	$\log \epsilon(X)$ [dex]	EW [mÅ]	$\log \epsilon(X)$ [dex]
5889.950	NaI	0.00	0.108	196.64	4.00	175.91	3.54	141.05	3.52	153.99	3.72	112.99	3.84	29.91	2.70
5895.924	NaI	0.00	–0.194	166.54	3.89	155.12	3.51	117.04	3.37	126.36	3.53	89.59	3.70	19.75	2.70
3829.355	MgI	2.71	–0.208	132.91	5.17	85.21	4.68
3986.753	MgI	4.35	–1.030	33.86	5.22	19.58	4.99	15.29	5.26
...															

(1999) and Alonso et al. (1996) calibrations. We chose $V - K$ since it is least affected by reddening. The reddening in the direction of each object was obtained from the dust maps of Schlegel et al. (1998) maps. However, it is known that these maps overpredict the reddening, in some cases quite significantly. Accordingly, different reddening correction were invoked, following the procedures of Bonifacio et al. (2000) and Meléndez & Asplund (2008). Temperatures were then calculated based on the two reddening estimates to investigate the impact of these reddening uncertainties. In a few cases, we adopted yet a different value. For HD140283, we also adopt $E(B - V) = 0.01$, following Ryan et al. (1996b), rather than $E(B - V) = 0.16$ from the dust maps. For HD122563, we also adopt $E(B - V) = 0.0$, following Honda et al. (2004).

We also find a strong relation between the difference in temperatures as a function of the initial spectro-

scopic temperatures, as can be seen in Figure 2 (bottom panel). The slope is even steeper because $V - K$ produces temperatures for giants that are warmer than what we adopted. Within the error bars, however, the slope of our main temperature comparison is still in rough agreement with what we determined based on $V - K$ colors. We note that this comparison only contains five of the seven sample stars. We had to exclude two stars (BD–18 5550 and G64–12) because their $V - K$ temperature were rather different (more than 200 K in the case of BD–18 5550) from what one would expect the temperatures of these stars to be, regardless of any employed method.

In the end we adopt the slope of our initial comparison because our overall aim is to adjust the spectroscopic temperatures to *average* photometric values. Even with photometry and color-temperature relations available, the temperatures derived from different colors often vary 100–200 K, as can be seen in Table 2. Finding a different slope based on the $V - K$ temperatures appears to reflect this dispersion.

We then turned the temperature differences from Figure 2 into values for the slope of the abundance trends to adopt in the FeI line abundance vs. excitation potential diagnostics. This is shown in Figure 3. In the top panel we show how the values of the slopes of the FeI line abundances after only correcting for the temperature and before adjusting the microturbulent velocity and the gravity. To guide the eye, we fit the data points with a second-order polynomial, which is also shown in the Figure. We estimate typical uncertainties in the slope to be 0.005 dex/eV or less.

For near main-sequence stars, the spectroscopic method delivers nearly the same temperatures as photometry, hence there is no significant slope of line abundances with excitation potential (~ 0.00 dex/eV). For the giants, however, applying significant temperature corrections according to Eq. (1) produces an initial slope of up to -0.09 dex/eV. We then carried out the remaining parts of the analysis: re-determining the microturbulent velocity and the surface gravity while ignoring the slope in the temperature diagnostic plot of line abundance vs. excitation potential. While the gravity was adjusted by up to ~ 0.7 dex for the most extreme cases, the microturbulent velocity decreased by less (~ 0.1 or less in most cases). The model metallicity $[m/H]$ was usually increased by about 0.1 to 0.2 dex following the increase in the Fe abundance.

Through the process of adjusting the remaining stellar parameters (gravity, microturbulent velocity, metallicity), we actually found that the slope of abundance with excitation potential was reduced. Figure 3 (bottom panel) shows the final slopes in the temperature

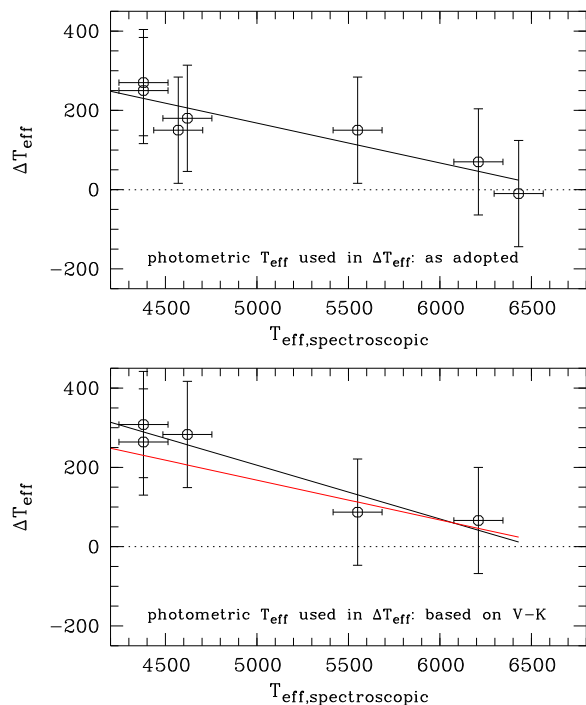


FIG. 2.— Differences in effective temperatures between our initial excitation temperatures and adopted literature photometry-based values (top panel) and those calculated from $V - K$ (bottom panel). We also show the slope from the top panel in the bottom panel (red line). The differences are most pronounced at the cooler temperatures of upper red giant branch stars, whereas main-sequence stars are hardly affected.

TABLE 2
EFFECTIVE TEMPERATURES COLLECTED FROM LITERATURE

T_{eff}	σ	Colors	Method	Reference	Comments
HD122563					
4670	28 ¹	V,J,K	COH78, FRO 83	Peterson et al. (1990)	phot. from NIC78, CAR83
4650	30 ²	B,V,R,I	BG78, BG89	Ryan et al. (1996b)	their phot., BN84, GS91
4572	61	IRFM	their calibration	Alonso et al. (1999)	as quoted in PASTEL database
4617	44 ¹	B,V,R,J,K	ALO99	Cayrel et al. (2004)	phot. from ALO98, BEE07, EPC99; adopt 4600
4546	75 ¹	B,V,K	ALO99	Honda et al. (2004)	phot. from Simbad; adopt 4570
4616	17 ¹	B,V,K,b,y	ALO99	Lai et al. (2004)	phot. from Simbad, HM98
4843	...	B,V,R,J,K	RM05	Yong et al. (2013)	phot. from CAY04, HON04
HE 1523–0901					
4630	40	B,V,R,I,J,H,K	ALO99	Frebel et al. (2007a)	phot. from BEE07
BD–18 5550					
4750	0 ¹	V,J,K	COH78, FRO83	Peterson et al. (1990)	phot. from CAR78, CAR83
4789	27 ¹	B,V,R	BG78, BG89	McWilliam et al. (1995)	their phot.
4668	...	IRFM	their calibration	Alonso et al. (1999)	as quoted in PASTEL database
4700	129 ¹	B,V,R,J,K	ALO99	Cayrel et al. (2004)	phot. from ALO98, BEE07, EPC99; adopt 4750
4558	...	B,V,R,J,K	RM05	Yong et al. (2013)	phot. from CAY04
CS 22892–052					
4763	54 ¹	B,V,R	BG78, BG89	McWilliam et al. (1995)	their phot.
4850	...	B,V	see RYA96b	Norris et al. (1997)	phot. from RYA89, BPS92, NOR97
4860	83 ¹	B,V,R,I,J,K	ALO99	Cayrel et al. (2004)	phot. from ALO98, BEE07, EPC99; adopt 4850
4740	69 ¹	B,V,K	ALO99	Honda et al. (2004)	adopt 4790
4825	...	B,V,R,J,K	RM05	Yong et al. (2013)	phot. from CAY04, HON04
HD140283					
5691	...	IRFM	their calibration	Alonso et al. (1996)	as quoted in HOS09
5640	...	V,R,I,K	their calibration	Bikmaev et al. (1996)	as quoted in MAS99
5750	50 ²	B,V,R,I	BO86, BK92	Ryan et al. (1996b)	their phot.
5750	53	V,J,K	HOU00	Cohen et al. (2002)	their phot.
5609	34 ¹	B,V,K	ALO96	Honda et al. (2004)	phot. from Simbad; adopt 5630
5751	50 ²	uvby- β	ALO96	Jonsell et al. (2005)	phot. from OLS83, SN88
5777	55	IRFM	their calibration	Casagrande et al. (2010)	
5711	...		CAS10	Yong et al. (2013)	phot. from COH02, HON04
CD–24 17504					
6060	54 ²	B,V,R,I,b,y	BO86, BK92, MAG87, VB85	Ryan et al. (1996a)	phot. from RYA89
6373	...	IRFM	their calibration	Alonso et al. (1996)	as quoted in PRI00b
6237	79 ^{1,3}	b,y	CAR83, KIN93	Primas et al. (2000b)	phot. from RYA99
6455	62	IRFM	their calibration	Casagrande et al. (2010)	
6236	...		CAS10	Yong et al. (2013)	phot. from RYA91
6290	...	V,R,I,J,K	CAS10	This Study	phot. from RYA91
G64–12					
6325	...	B,V,R,I,b,y	BUS87, BO86, KUR89, MAG87, VB85	Ryan et al. (1991)	phot. from RYA89, SN88, CAR83, this work
6290	44 ²	B,V,R,I,b,y	BO86, BK92, MAG87, VB85	Ryan et al. (1996a)	phot. from CAR78, CAR89, CS92, SN89, SCH93
6470	90	IRFM	their calibration	Alonso et al. (1996)	as quoted in PRI00a
6430	75 ¹	B,V,R,I,K	ALO96	Aoki et al. (2006)	
6464	61		IRFM	their calibration	CAS10
6450	35 ¹	B,V,R,I,K	CAS10	This Study	phot. from AOK06 colors

NOTE. — JHK magnitudes were used in many of the cited studies and most are taken from 2MASS (Skrutskie et al. 2006). References for photometry and color-temperature relations: ALO96 – Alonso et al. (1996); ALO98 – Alonso et al. (1998); ALO99 – Alonso et al. (1999); AOK06 – Aoki et al. (2006); BO86 – Bell & Oke (1986); BEE07 – Beers et al. (2007); BG78 – Bell & Gustafsson (1978); BG89 – Bell & Gustafsson (1989); BK92 – Buser & Kurucz (1992); BN84 – Bessell & Norris (1984); BPS92 – Beers et al. (1992); BUS87 – Buser, private communication in Ryan et al. (1991); BK92 – Buser & Kurucz (1992); CAR78 – Carney (1978); CAR83 – Carney (1983); CAR89 – Carney et al. (1989); CAS10 – Casagrande et al. (2010); CAY04 – Cayrel et al. (2004); CS92 – Cayrel de Strobel et al. (1992); COH78 – Cohen et al. (1978); COH02 – Cohen et al. (2002); EPC99 – (Epchtein et al. 1999); FRO83 – Frogel et al. (1983); GS91 – Gratton & Snenen (1991); HM98 – Hauck & Mermilliod (1998); HOU00 – Houdashelt et al. (2000); HON04 – Honda et al. (2004); HOS09 – Hosford et al. (2009); KIN93 – King (1993); KUR89 – Kurucz, private communication in Ryan et al. (1991); MAG87 – Magain (1987); MAS99 – Mashonkina et al. (1999); NIC78 – Nicolet (1978); NOR97 – Norris et al. (1997); OLS83 – Olsen (1983); PASTEL – Soubiran et al. (2010); PRI00a – Primas et al. (2000a); PRI00b – Primas et al. (2000b); RM05 – Ramirez & Meléndez (2005); RYA89 – Ryan (1989); RYA91 – Ryan et al. (1991); RYA96b – Ryan et al. (1996b); RYA99 – Ryan et al. (1999); SN88 – Schuster & Nissen (1988); SN89 – Schuster & Nissen (1989); SCH93 – Schuster et al. (1993); VB85 – Vandenberg & Bell (1985)

¹ Standard deviations of the average temperatures (column 1) calculated from the different colors (column 3).

² Error based on assessment of errors in photometry/reddening.

³ Average of values from two different color- T_{eff} relation.

TABLE 3
 STELLAR PARAMETERS OF THE SAMPLE

Star	$T_{\text{eff,adop.}}$ [K]	$T_{\text{eff,V-K}}$ [K]	initial determination				after temperature correction			
			T_{eff} [K]	$\log(g)$ [dex]	[Fe/H] [dex]	v_{micr} [km s ⁻¹]	T_{eff} [K]	$\log(g)$ [dex]	[Fe/H] [dex]	v_{micr} [km s ⁻¹]
HD122563	4650	4644	4380	0.10	-2.93	2.65	4612	0.85	-2.79	2.30
HE 1523-0901	4630	4688	4380	0.05	-2.97	2.85	4612	0.80	-2.85	2.70
BD -18 5550	4720	...	4570	0.80	-3.20	2.05	4783	1.25	-3.02	2.00
CS22892-052	4800	4903	4620	0.85	-3.24	2.20	4828	1.35	-3.08	2.15
HD140283	5700	5637	5550	2.95	-2.74	1.50	5665	3.20	-2.64	1.45
CD -24 17504	6280	6276	6210	3.60	-3.26	1.35	6259	3.65	-3.23	1.40
G64-12	6420	...	6430	4.35	-3.30	1.45	6457	4.40	-3.28	1.50

diagnostic plots. The most extreme one is now only -0.07 dex/eV which, in the end, only corresponds to a temperature difference of 150 K compared to a slope of 0.000 dex/eV. However, we caution that if one would change the temperature again to produce no trend, the gravity and microturbulent velocity would change again, and one would once again iterate towards the lower temperature/lower gravity/higher microturbulent velocity solution. Regardless, 150 K is of the same order as what uncertainties in spectroscopic effective temperatures generally are. It is thus reassuring that despite of applying our temperature corrections, we are producing temperatures that nominally are no more than 150 K away from a trend with no slope. Table 3 shows the initial and corrected final sets of stellar parameters of all sample stars.

In Figure 4, we show the FeI line abundances as a function of excitation potential for all sample stars. Plotted are the line abundances showing no trend of excitation potential as initially derived and the final line abundances after temperature correction and subsequent adjustment of v_{mic} and $\log g$. This illustrates how the slope changes as a result of our analysis, which is also quantified in the two panels in Figure 3.

We then checked how the initial and corrected sets of stellar parameters compare with an isochrone. We used 12 Gyr isochrones with $[\text{Fe}/\text{H}] = -3.0, -2.5$ and -2.0 and α -enhancement of $[\alpha/\text{Fe}] = 0.3$ (Kim et al. 2002). Figure 5 shows the results. The initial, too cool temper-

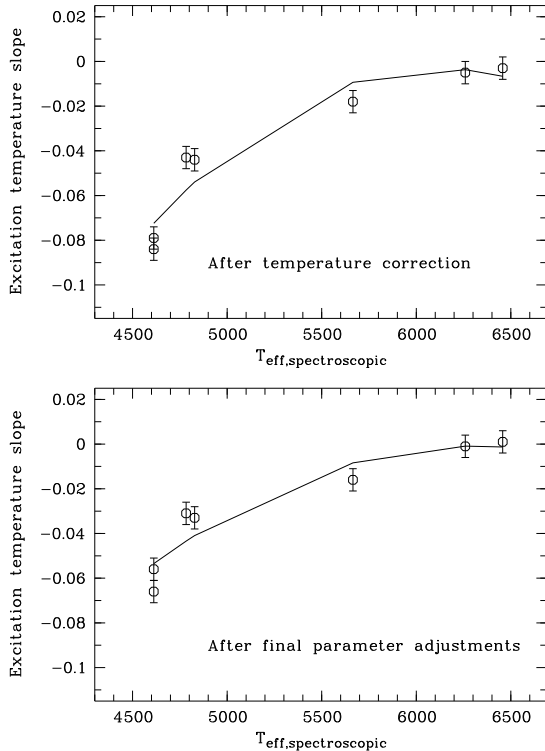


FIG. 3.— The slopes of the FeI line abundances as a function of their excitation potentials after only adjusting the temperature according to our method (top panel) and after also adjusting the surface gravity and microturbulent velocity (bottom panel) to arrive at the final stellar parameters. The maximum slope in the bottom panel nominally corresponds to ~ 150 K compared with a slope of 0.000 dex/eV.

atures pushed the giants off the isochrones at < 4500 K. The corrected values agree very well with the isochrones. The only small exception is the subgiant HD140283, which is ~ 0.3 dex off the subgiant branch or 250 K from the base of the giant branch. However, the initial stellar parameters made this star more of a warm giant rather than a subgiant. Hence, the corrected stellar parameters provide better solution for this star.

Finally, we checked how the microturbulent velocities as a function of the surface gravity compare with those of other studies. In Figure 6 we compare our values with those of Cayrel et al. (2004) and Barklem et al. (2005) who used photometrically determined temperatures for their studies. There exists some scatter in the microturbulent velocities for a given gravity within each study and perhaps also some small systematic difference. While the Cayrel et al. values have been derived with the same methodology as used in this study, the Barklem et al. values are derived from synthesizing spectral lines by simultaneously solving for all four stellar parameters (although based on appropriate initial guesses). Table 3 of Barklem et al. (2005) suggests that with this technique slightly higher surface gravities and higher microturbulent velocities (0.1 to 0.3 km s^{-1}) are derived, compared to other literature studies. Assuming typical uncertainties of 0.3 km s^{-1} our microturbulent velocities are in good agreement with those from the literature.

Based on the properties of our chosen sample of stars, this method has been accurate for metal-poor subgiants and giants with $-3.3 < [\text{Fe}/\text{H}] < -2.5$ that have high-resolution spectra with a large wavelength coverage (at least 4750 to 6800 Å).

We carried out further tests to assess the validity of our adjustment scheme at $[\text{Fe}/\text{H}] < -3.5$. As part of this we analyzed CD-38 245 ($[\text{Fe}/\text{H}] = -4.2$; e.g., Yong et al. 2013), HE 1300+0157 ($[\text{Fe}/\text{H}] = -3.7$; Frebel et al. 2007b), HE 0557-4840 ($[\text{Fe}/\text{H}] = -4.8$; Norris et al. 2007), HE 0107-5240 ($[\text{Fe}/\text{H}] = -5.4$; Christlieb et al. 2002), and HE 1327-2326 ($[\text{Fe}/\text{H}] = -5.6$; Frebel et al. 2005). In all cases, we found that the excitation temperatures yield much lower values (ΔT_{eff} of 500 to 1400 K) for these ultra metal-poor stars than what was found for our sample of seven extremely metal-poor stars (the maximal ΔT_{eff} is 270 K, see Figure 2). Hence, we speculate that at $[\text{Fe}/\text{H}] < -3.5$ the excitation method to determine effective temperatures may not be sufficient for the task, perhaps because of (metallicity dependent) effects, such as NLTE effects or the accuracy of model atmospheres (e.g. plane-parallel models for cooler, extended giants), or simply because at those metallicities, only relatively few Fe lines are available from the spectra. While we used all known stars with $[\text{Fe}/\text{H}] < -4.0$ that had published equivalent widths, the number of stars remains small, and our individual ΔT_{eff} values should perhaps be regarded as somewhat anecdotal. In summary, we suggest that our calibration appears to be breaking down at $[\text{Fe}/\text{H}] \sim -4.0$.

We also tested if any of our results would change if fewer blue lines would be available due to the use of spectrographs other than MIKE on Magellan or Xshooter on VLT that yield (nearly) full optical coverage. Mimicking a Subaru/HDS two-arm setting (4000 to 6800 Å) and the VLT/UVES 580nm setting (4750 to 6800 Å), we checked

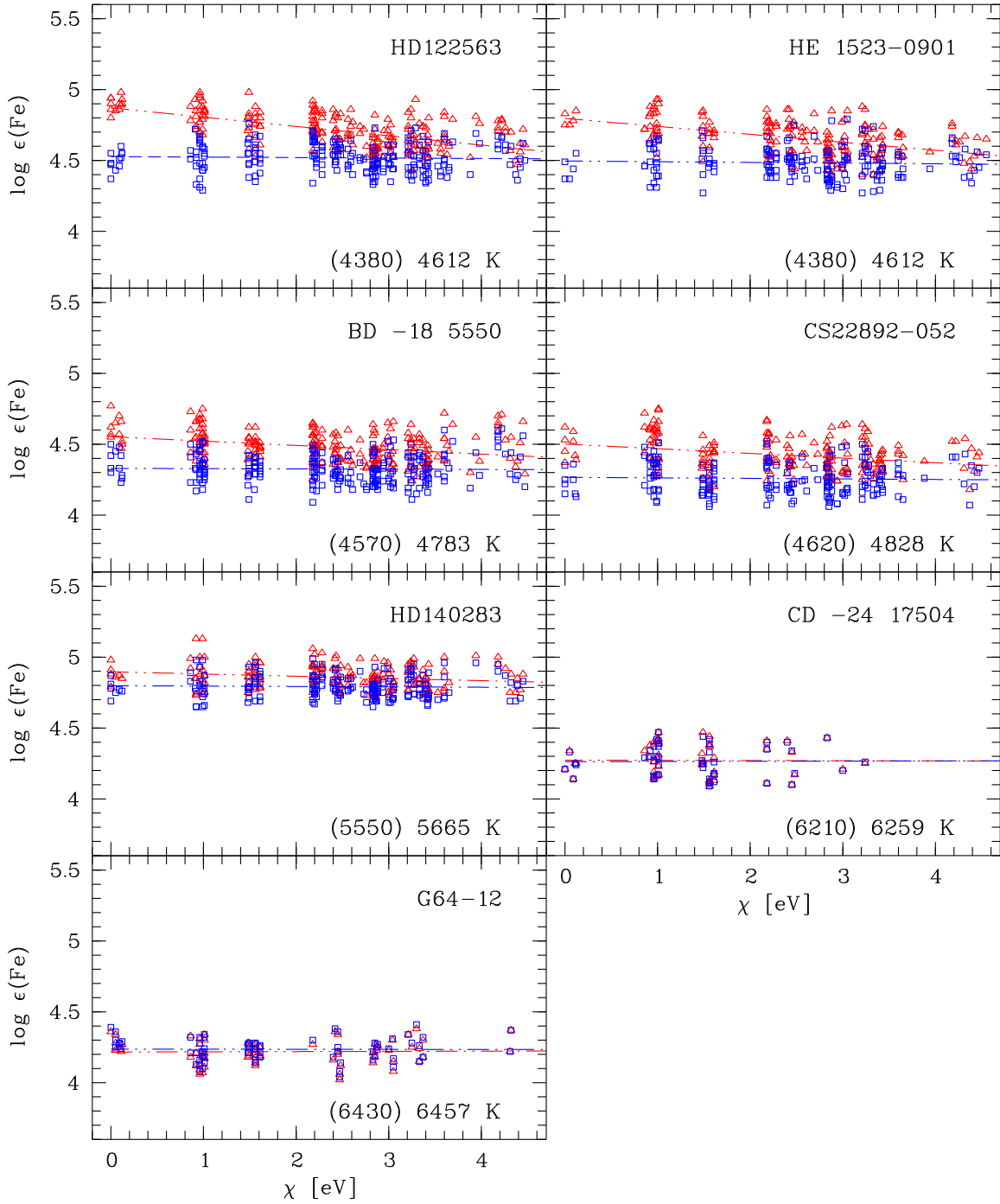


FIG. 4.— Fe I line abundances as a function of excitation potential χ for all sample stars. Plotted are the line abundances showing no trend of excitation potential as initially derived (blue squares), and the final line abundance trends following the temperature adjustment and after v_{mic} , $\log g$ and metallicity have been adjusted (red triangles). Shown also are the corresponding initial (in brackets) and final temperature.

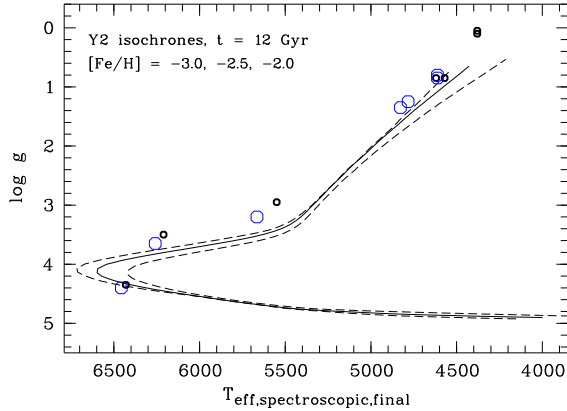


FIG. 5.— Our initial (small black open circles) and corrected stellar parameters (larger open blue circles) plotted over 12 Gyr isochrones with $[\text{Fe}/\text{H}] = -3.0$, $[\text{Fe}/\text{H}] = -2.5$ and $[\text{Fe}/\text{H}] = -2.0$, all having an α -enhancement of $[\alpha/\text{Fe}] = 0.3$ (Kim et al. 2002). The agreement of the stellar parameters with the isochrones following the temperature adjustment is very good. The cooler giants do not extend past the upper red giant branch of the isochrones anymore.

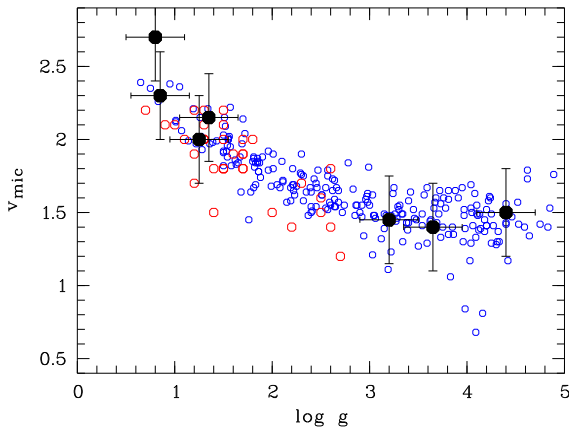


FIG. 6.— Final microturbulent velocities as function of the surface gravity for the sample stars (black filled circles) as well as the Cayrel et al. (2004) sample (small red circles) and Barklem et al. (2005) sample (without the horizontal branch stars; small blue circles).

whether using reduced wavelength ranges would change our stellar parameters. Only small changes were found. Temperatures changed by up to 40 K (making the stars warmer, although not in all cases) and the microturbulent velocity changed between 0.05 and 0.3 km s^{-1} . The main concern with this exercise was to have sufficient number of Fe I lines (between 50 and 150) and Fe II lines (more than at least 2 to 3) available, many of which (especially Fe II) are located between 4400 and 4650 Å. Hence, for the near main-sequence turn-off stars cutting at 4750 Å did not yield well-determined stellar parameters since only 20 (for G64-12) and 6 (for CD-24 17504) Fe I and only 2 Fe II (both stars) were available.

Finally, we note that any line abundance corrections based on line formation under non-local thermodynamic equilibrium (NLTE) would increase the surface gravity. We made a test where we assumed a simple average correction for Fe I of 0.2 dex, and assuming that NLTE does

not affect Fe II (e.g., Asplund 2005). This increases the gravity of about 0.5 dex. Such a large change might be welcome for the cooler giants when not applying our adjustments, i.e. in combination with the too cool temperatures that result in too low gravities, but for near-main-sequence stars a large gravity increase would pose problems regardless. More detailed stellar parameter determination techniques seem to be required to resolve this issue (e.g. Bergemann et al. 2012; Lind et al. 2012).

4. METAL ABUNDANCE RESULTS AND COMPARISON WITH LITERATURE VALUES

For completeness, we present the chemical abundances of our sample stars in Table 4. Solar abundances are taken from Asplund et al. (2009). We note that while for the Fe abundances we employed only lines with wavelengths longer than 3700 Å, but for a few other elements (Ti, Cr, Ni) we also included a few lines at shorter wavelengths for better statistics whenever they were measurable. For each star, we also compared the abundances with those of another study from the literature (Norris et al. 2001; Honda et al. 2004; Cayrel et al. 2004; Aoki et al. 2006). We chose those studies because they yielded stellar parameters for a given star that agreed well with our results. We took the abundances from Frebel (2010) to ensure that all studies employ the same solar abundances. The stellar abundance differences in the final $[\text{X}/\text{Fe}]$ values between our and the literature studies are reasonable and typically within 0.2 dex.

Table 5 lists stellar parameters for an additional five stars from the sample of Cayrel et al. (2004) for which we also had Magellan/MIKE spectra. We used these stars to further test our method and stellar parameter determination technique. Furthermore, we add three of our sample stars (HD122563, BD -18 5550, CS22892-052) because they are also part of the Cayrel et al. sample. This allows us to compare our stellar parameters with the Cayrel et al. results as well as with those of Yong et al. (2013) who analyzed the Cayrel et al. stars as part of a sample of 190 metal-poor stars from the literature. Figure 7 illustrates the results and shows the good agreement of our effective temperature and surface gravity compared to the photometrically derived temperatures and gravities (also derived from the Fe I-Fe II ionization equilibrium) by Cayrel et al. (2004) (top panel) and Yong et al. (2013) (bottom panel).

The only star for which we determine very different stellar parameters than Cayrel et al. (2004) and Yong et al. (2013) is CS30325-094. We find its corrected temperature to be about 340 K cooler. A simple check of the shape of the Balmer lines in comparison with the stars from our sample suggests the star to be not warmer than 4800 K (on our adjusted scale). This remains in contrast with what has been found from photometry.

A similar, albeit less severe case, is HD2796. Our corrected temperature is about 100 K cooler, but this star also has a somewhat higher metallicity ($[\text{Fe}/\text{H}] \sim -2.5$). If the differences between excitation temperatures and photometric temperatures was less severe for giants at higher metallicity, this could explain the discrepant temperature. However, both our initial and final stellar parameter solutions as well as that of Cayrel et al. (2004) do not match any position of the red giant branch on the isochrone. Rather, the star sits slightly above it,

TABLE 4
MAGELLAN/MIKE CHEMICAL ABUNDANCES OF THE SAMPLE STARS

Species	HD122563				HE 1523-0901				BD -18 5550				CS22892-052			
	$\lg \epsilon(X)$	[X/Fe]	N	σ	$\lg \epsilon(X)$	[X/Fe]	N	σ	$\lg \epsilon(X)$	[X/Fe]	N	σ	$\lg \epsilon(X)$	[X/Fe]	N	σ
Na I	3.95	0.50	2	0.05	3.52	0.13	2	0.02	3.45	0.23	2	0.07	3.62	0.46	2	0.10
Mg I	5.26	0.45	7	0.07	5.08	0.33	6	0.09	4.99	0.41	7	0.06	4.85	0.33	5	0.09
Si I	5.17	0.45	3	0.06	5.09	0.43	1	0.00	4.90	0.41	1	0.00	5.05	0.62	1	0.00
Ca I	3.87	0.32	25	0.08	3.78	0.29	21	0.08	3.72	0.40	25	0.08	3.66	0.39	18	0.08
Sc I	0.42	0.07	13	0.07	0.27	-0.03	12	0.08	0.17	0.04	9	0.06	0.03	-0.04	6	0.07
Ti I	2.28	0.12	31	0.07	2.26	0.16	26	0.09	2.15	0.22	28	0.09	2.07	0.19	13	0.09
Ti II	2.37	0.21	51	0.10	2.35	0.24	41	0.11	2.16	0.23	49	0.11	2.10	0.22	36	0.10
Cr I	2.56	-0.29	21	0.08	2.65	-0.15	14	0.11	2.43	-0.19	20	0.03	2.26	-0.30	10	0.06
Cr II	2.89	0.04	3	0.05	3.12	0.32	2	0.12	2.73	0.11	3	0.05	2.45	-0.11	1	0.00
Fe I	4.71	0.00	222	0.12	4.65	0.00	183	0.12	4.48	0.00	233	0.11	4.42	0.00	191	0.12
Fe II	4.72	0.01	26	0.10	4.65	-0.00	25	0.13	4.49	0.01	24	0.08	4.44	0.01	21	0.10
Co I	2.42	0.22	6	0.10	2.49	0.34	4	0.20	2.24	0.27	8	0.10	2.20	0.29	7	0.10
Ni I	3.56	0.13	24	0.08	3.40	0.03	17	0.09	3.35	0.15	22	0.11	3.36	0.22	11	0.09
Zn I	1.92	0.15	2	0.04	1.92	0.20	2	0.04	1.86	0.33	2	0.05	2.06	0.58	1	0.00

Species	HD140283				CD-24 17504				G64-12			
	$\lg \epsilon(X)$	[X/Fe]	N	σ	$\lg \epsilon(X)$	[X/Fe]	N	σ	$\lg \epsilon(X)$	[X/Fe]	N	σ
Na I	3.77	0.17	2	0.07	2.73	-0.28	2	0.03	2.90	-0.06	2	0.04
Mg I	5.26	0.30	9	0.07	4.75	0.38	5	0.08	4.70	0.38	6	0.09
Si I	5.41	0.54	2	0.03	4.40	0.12	1	0.00	4.52	0.29	1	0.00
Ca I	4.00	0.30	20	0.07	3.32	0.21	3	0.06	3.58	0.52	13	0.08
Sc I	0.54	0.03	7	0.05	0.21	0.29	1	0.00	0.17	0.30	1	0.00
Ti I	2.55	0.25	20	0.08	3.12	1.40	2	0.02	0	...
Ti II	2.52	0.21	44	0.08	1.85	0.13	9	0.06	2.18	0.51	14	0.07
Cr I	2.83	-0.17	14	0.07	2.26	-0.15	5	0.06	2.22	-0.14	6	0.08
Cr II	3.09	0.09	3	0.08	2.71	0.30	1	0.00	0	...
Fe I	4.86	0.00	185	0.08	4.27	0.00	49	0.11	4.22	0.00	70	0.08
Fe II	4.87	0.01	19	0.07	4.29	0.01	2	0.02	4.24	0.02	3	0.01
Co I	2.59	0.24	6	0.05	2.48	0.72	3	0.05	2.17	0.46	2	0.02
Ni I	3.77	0.20	22	0.08	3.33	0.33	7	0.09	3.19	0.25	10	0.09
Zn I	2.05	0.14	2	0.05	0	0	...

NOTE. — [X/Fe] abundance ratios are computed with [Fe/H] abundances of the respective stars. Solar abundances have been taken from Asplund et al. (2009). The uncertainties listed are standard deviations of the line abundances for each element. Standard errors for each abundance will be much smaller. For abundances measured from only one line, we adopt a nominal uncertainty of 0.10 dex.

perhaps suggesting that the star is descending onto the horizontal branch. However, Yong et al. (2013) do find a gravity that that matches the isochrone. Again, the shape of the Balmer lines suggest a cooler temperature than the photometrically derived temperatures.

5. CONCLUSION

We have presented a straight-forward method to adjust spectroscopic temperatures that have been derived from Fe I line abundances as a function of their excitation potential. The main aim was to avoid obtaining too cool spectroscopic temperatures especially for upper red giant branch stars that are often several hundred degrees cooler than photometrically derived temperatures. A pleasant side effect of this temperature adjustment is that higher surface gravities are obtained and artificially high microturbulent velocities are avoided. Overall this brings the fully spectroscopic, reddening independent stellar parameters in agreement with photomet-

rically derived ones, and also with isochrones of the respective stellar metallicities. While the stellar sample is based on stars with $-3.3 < [\text{Fe}/\text{H}] < -2.5$, additional tests indicate that our adjustment scheme is not usable for stars with $[\text{Fe}/\text{H}] < -4.0$.

We tested our method with additional stars from the Cayrel et al. (2004) sample that were also analyzed by Yong et al. (2013) and generally found agreement to within ~ 50 K. The results of applying the new temperature determination method to new samples of extremely metal-poor stars will be reported in a forthcoming paper.

A.R.C. acknowledges the financial support through the Australian Research Council Laureate Fellowship 0992131, and from the Australian Prime Minister's Endeavour Award Research Fellowship, which has facilitated his research at MIT. This research has made use of the SIMBAD database, operated at CDS, Strasbourg, France and of NASA's Astrophysics Data System Bibliographic Services.

Facilities: Magellan-Clay (MIKE)

REFERENCES

- Alonso, A., Arribas, S., & Martínez-Roger, C. 1996, *A&A*, 313, 873
—, 1998, *A&AS*, 131, 209
Alonso, A., Arribas, S., & Martínez-Roger, C. 1999, *A&As*, 140, 261
Aoki, W., Arimoto, N., Sadakane, K., et al. 2009, *A&A*, 502, 569
Aoki, W., Frebel, A., Christlieb, N., et al. 2006, *ApJ*, 639, 897
Aoki, W., Honda, S., Beers, T. C., et al. 2007, *ApJ*, 660, 747
Asplund, M. 2005, *ARA&A*, 43, 481
Asplund, M., Grevesse, N., Sauval, A. J., & Scott, P. 2009, *ARA&A*, 47, 481
Barklem, P. S., Christlieb, N., Beers, T. C., et al. 2005, *A&A*, 439, 129
Barklem, P. S., Stempels, H. C., Allende Prieto, C., et al. 2002, *A&A*, 385, 951
Beers, T. C., Flynn, C., Rossi, S., et al. 2007, *ApJS*, 168, 128
Beers, T. C., Preston, G. W., & Shectman, S. A. 1992, *AJ*, 103, 1987

TABLE 5
 STELLAR PARAMETERS OF A TEST SAMPLE

Star	T_{eff} [K]	$\log(g)$ [dex]	[Fe/H] [dex]	v_{micr} [km s $^{-1}$]
initial determination				
CS22873-166	4350	0.10	-3.02	2.70
HD122563	4380	0.10	-2.93	2.65
CS30325-094	4380	0.40	-3.90	2.40
HD186478	4520	0.60	-2.64	2.10
CD-38 245	4500	0.85	-4.28	2.05
BD-18 5550	4570	0.80	-3.20	2.05
CS31082-001	4640	1.25	-3.00	2.25
CS22892-052	4620	0.85	-3.24	2.20
HD2796	4660	0.45	-2.65	2.35
after temperature correction				
CS22873-166	4585	0.90	-2.90	2.60
HD122563	4612	0.85	-2.79	2.30
CS30325-094	4612	1.05	-3.70	2.15
HD186478	4738	1.30	-2.50	2.15
CD-38 245	4720	1.40	-4.06	1.95
BD-18 5550	4783	1.25	-3.02	2.00
CS31082-001	4846	1.70	-2.82	2.25
CS22892-052	4828	1.35	-3.08	2.15
HD2796	4864	1.00	-2.50	2.25
Cayrel et al. (2004)				
CS22873-166	4550	0.90	-2.97	2.10
HD122563	4600	1.10	-2.82	2.10
CS30325-094	4950	1.50	-3.30	2.00
HD186478	4700	1.30	-2.59	2.00
CD-38 245	4800	1.50	-4.19	2.20
BD-18 5550	4750	1.40	-3.06	1.80
CS31082-001	4825	1.80	-2.91	1.50
CS22892-052	4850	1.60	-3.03	1.90
HD2796	4950	2.10	-2.47	1.50
Yong et al. (2013)				
CS22873-166	4516	0.77	-2.74	1.60
HD122563	4843	1.62	-2.54	1.80
CS30325-094	4948	1.85	-3.35	1.60
HD186478	4629	1.07	-2.68	2.00
CD-38 245	4857	1.54	-4.15	2.20
BD-18 5550	4558	0.81	-3.20	1.70
CS31082-001	4866	1.66	-2.75	1.40
CS22892-052	4825	1.54	-3.03	1.60
HD2796	4923	1.84	-2.31	1.60

NOTE. — The original abundance from Cayrel et al. (2004) have been redetermined using the solar abundances from Asplund et al. (2009).

Bell, R. A., & Gustafsson, B. 1978, *A&AS*, 34, 229
 —. 1989, *MNRAS*, 236, 653
 Bell, R. A., & Oke, J. B. 1986, *ApJ*, 307, 253
 Bergemann, M., Lind, K., Collet, R., Magic, Z., & Asplund, M. 2012, *MNRAS*, 427, 27
 Bernstein, R., Shectman, S. A., Gunnels, S. M., Mochnacki, S., & Athey, A. E. 2003, in *Society of Photo-Optical Instrumentation Engineers (SPIE) Conference Series*, ed. M. Iye & A. F. M. Moorwood, Vol. 4841, 1694
 Bessell, M. S. 2007, *PASP*, 119, 605
 Bessell, M. S., & Norris, J. 1984, *ApJ*, 285, 622
 Bikmaev, I. E., Mashonkina, L. I., Sakhbullin, N. A., Shimanskij, V. V., & Shimanskaya, N. 1996, in *IAU Symposium*, Vol. 169, *Unsolved Problems of the Milky Way*, ed. L. Blitz & P. J. Teuben, 389
 Bonifacio, P., Monai, S., & Beers, T. C. 2000, *AJ*, 120, 2065
 Buser, R., & Kurucz, R. L. 1992, *A&A*, 264, 557
 Carney, B. W. 1978, *AJ*, 83, 1087
 —. 1983, *AJ*, 88, 610
 Carney, B. W., Latham, D. W., & Laird, J. B. 1989, *AJ*, 97, 423
 Casagrande, L., Ramírez, I., Meléndez, J., Bessell, M., & Asplund, M. 2010, *A&A*, 512, 54
 Castelli, F., & Kurucz, R. L. 2004, arXiv:astro-ph/0405087
 Cayrel, R., Depagne, E., Spite, M., et al. 2004, *A&A*, 416, 1117
 Cayrel de Strobel, G., Hauck, B., Francois, P., et al. 1992, *A&AS*, 95, 273
 Christlieb, N., Bessell, M. S., Beers, T. C., et al. 2002, *Nature*, 419, 904

Cohen, J. G., Christlieb, N., Beers, T. C., Gratton, R., & Carretta, E. 2002, *AJ*, 124, 470
 Cohen, J. G., Christlieb, N., McWilliam, A., et al. 2008, *ApJ*, 672, 320
 Cohen, J. G., Persson, S. E., & Frogel, J. A. 1978, *ApJ*, 222, 165
 Epchtein, N., Deul, E., Derriere, S., et al. 1999, *A&A*, 349, 236
 Frebel, A. 2010, *Astronomische Nachrichten*, 331, 474
 Frebel, A., Aoki, W., Christlieb, N., et al. 2005, *Nature*, 434, 871
 Frebel, A., Christlieb, N., Norris, J. E., et al. 2007a, *ApJ*, 660, L117
 Frebel, A., Norris, J. E., Aoki, W., et al. 2007b, *ApJ*, 658, 534
 Frebel, A., Simon, J. D., Geha, M., & Willman, B. 2010, *ApJ*, 708, 560
 Frogel, J. A., Persson, S. E., & Cohen, J. G. 1983, *ApJS*, 53, 713
 Gratton, R. G., & Sneden, C. 1991, *A&A*, 241, 501
 Hauck, B., & Mermilliod, M. 1998, *A&AS*, 129, 431
 Hollek, J. K., Frebel, A., Roederer, I. U., et al. 2011, *ApJ*, 742, 54
 Honda, S., Aoki, W., Kajino, T., et al. 2004, *ApJ*, 607, 474
 Hosford, A., Ryan, S. G., García Pérez, A. E., Norris, J. E., & Olive, K. A. 2009, *A&A*, 493, 601
 Houdashelt, M. L., Bell, R. A., & Sweigart, A. V. 2000, *AJ*, 119, 1448
 Johnson, J. A. 2002, *ApJS*, 139, 219
 Jonsell, K., Edvardsson, B., Gustafsson, B., et al. 2005, *A&A*, 440, 321
 Kim, Y.-C., Demarque, P., Yi, S. K., & Alexander, D. R. 2002, *ApJS*, 143, 499
 King, J. R. 1993, *AJ*, 106, 1206
 Koch, A., McWilliam, A., Grebel, E. K., Zucker, D. B., & Belokurov, V. 2008, *ApJ*, 688, L13
 Lai, D. K., Bolte, M., Johnson, J. A., et al. 2008, *ApJ*, 681, 1524
 Lai, D. K., Bolte, M., Johnson, J. A., & Lucatello, S. 2004, *AJ*, 128, 2402
 Lind, K., Bergemann, M., & Asplund, M. 2012, *MNRAS*, 427, 50

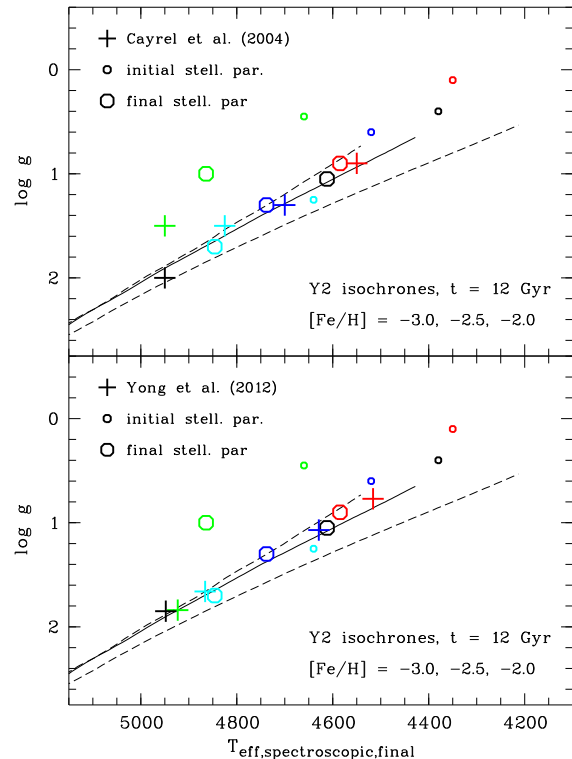


FIG. 7.— Initial (small open circles), corrected (larger open circles) stellar parameters compared with literature values (crosses) of Cayrel et al. (2004) (top panel) and Yong et al. (2013) (bottom panel). Color code: green: HD2796, red: CS22873-166, black: CS30325-094, blue: HD186478, cyan: CS31082-001. Overplotted are 12 Gyr isochrones with $[\text{Fe}/\text{H}] = -3.0$, $[\text{Fe}/\text{H}] = -2.5$ and $[\text{Fe}/\text{H}] = -2.0$ (from left to right), all having an α -enhancement of $[\alpha/\text{Fe}] = 0.3$ (Kim et al. 2002). See text for discussion.

- Magain, P. 1987, *A&A*, 179, 176
- Mashonkina, L., Gehren, T., & Bikmaev, I. 1999, *A&A*, 343, 519
- McWilliam, A., Preston, G. W., Sneden, C., & Searle, L. 1995, *AJ*, 109, 2757
- Meléndez, J., & Asplund, M. 2008, *A&A*, 490, 817
- Nicolet, B. 1978, *A&AS*, 34, 1
- Norris, J. E., Christlieb, N., Korn, A. J., et al. 2007, *ApJ*, 670, 774
- Norris, J. E., Ryan, S. G., & Beers, T. C. 1997, *ApJ*, 488, 350
- Norris, J. E., Ryan, S. G., & Beers, T. C. 2001, *ApJ*, 561, 1034
- Olsen, E. H. 1983, *A&AS*, 54, 55
- Peterson, R. C., Kurucz, R. L., & Carney, B. W. 1990, *ApJ*, 350, 173
- Primas, F., Asplund, M., Nissen, P. E., & Hill, V. 2000a, *A&A*, 364, L42
- Primas, F., Molaro, P., Bonifacio, P., & Hill, V. 2000b, *A&A*, 362, 666
- Ramírez, I., & Meléndez, J. 2005, *ApJ*, 626, 465
- Roederer, I. U., Sneden, C., Thompson, I. B., Preston, G. W., & Shectman, S. A. 2010, *ApJ*, 711, 573
- Ryan, S. G. 1989, *AJ*, 98, 1693
- Ryan, S. G., Beers, T. C., Deliyannis, C. P., & Thorburn, J. A. 1996a, *ApJ*, 458, 543
- Ryan, S. G., Norris, J. E., & Beers, T. C. 1996b, *ApJ*, 471, 254
- . 1999, *ApJ*, 523, 654
- Ryan, S. G., Norris, J. E., & Bessell, M. S. 1991, *AJ*, 102, 303
- Schlegel, D. J., Finkbeiner, D. P., & Davis, M. 1998, *ApJ*, 500, 525
- Schuster, W. J., & Nissen, P. E. 1988, *A&As*, 73, 225
- . 1989, *A&A*, 222, 69
- Schuster, W. J., Parrao, L., & Contreras Martinez, M. E. 1993, *A&AS*, 97, 951
- Simon, J. D., Frebel, A., McWilliam, A., Kirby, E. N., & Thompson, I. B. 2010, *ApJ*, 716, 446
- Skrutskie, M. F., Cutri, R. M., Stiening, R., et al. 2006, *AJ*, 131, 1163
- Sneden, C. A. 1973, PhD thesis, The University of Texas at Austin
- Sobeck, J. S., Kraft, R. P., Sneden, C., et al. 2011, *AJ*, 141, 175
- Soubiran, C., Le Campion, J.-F., Cayrel de Strobel, G., & Caillo, A. 2010 *A&A*, 515, 111
- Vandenbergh, D. A., & Bell, R. A. 1985, *ApJS*, 58, 561
- Yong, D., Norris, J. E., Bessell, M. S., et al. 2013, *ApJ*, 762, 26